NANO · MICRO small
www.small-journal.com

Multifaceted Cargo Recruitment and Release from Artificial Membraneless Organelles

*Jianhui Liu, Fariza Zhorabek, Tianfu Zhang, Jacky W. Y. Lam, Ben Zhong Tang, and Ying Chau**

Liquid-liquid phase separation (LLPS) drives membraneless organelles (MLOs) formation for organizing biomolecules. Artificial MLOs (AMLOs) have been constructed mostly via the LLPS of engineered proteins capable of regulating limited types of biomolecules. Here, leveraging a minimalist AMLO, driven by LLPS of polymer-oligopeptide hybrids, enrichment, recruitment, and release of multifaceted cargoes are quantitatively shown, including small fluorescent molecules, fluorophore-containing macromolecules, proteins, DNAs, and RNAs. Cargoes show up to 10^5-fold enrichment, whilst recruitment and release are triggered by variations of temperature, pH, and/or ionic strength. Also, the first efficacious, rapid, and reversible control of aggregation-induced emission with over 30 folds of modulation of overall fluorescence intensity is achieved, by intensifying the aggregation of luminogens in AMLO. The AMLO is a simple yet versatile platform for potential drug delivery and biosensor applications.

1. Introduction

Intracellular functioning demands precise spatiotemporal regulation of myriad biomolecules by virtue of compartmentalization, canonically via the formation of lipid bilayer membrane-bound organelles.[1] Nonetheless, the formation of membraneless organelles[2] (MLOs) was revealed as another universal organization method, enabled by liquid-liquid phase separation (LLPS).[3] Millions of biomolecules[4] exist within MLOs, spanning over a wide range of nature, including small cargo molecules,[5] proteins,[6] DNAs,[7] and RNAs.[8,9] They can be broadly classified into two categories, "scaffolds" and "clients," which are essential and dispensable for the formation[10] of MLOs, respectively. In particular, intrinsically disordered proteins (IDPs) are the major scaffold molecules.[11] Construction of simplified model MLOs with well-defined interaction modules has aroused intense interest for the elucidation of complex biological principles[12] and for the development of biosystems with designer functions.[13,14] Distinctive from the common method to reconstitute MLOs from genetically engineered IDPs, we recently reported a minimalist design of IDP-mimicking polymer-oligopeptide hybrid (IPH). IPH*, which is designed to mimic FUS protein, phase separated to form artificial MLOs, which could preferentially enrich green fluorescence protein and model RNAs in the interior.[15,16] The liquid nature of artificial MLO (AMLO) is ideal for the hosting and preservation of biological molecules, affording the possibility of sensing, as well as fast, adaptive, and reversible responses to various stimuli (e.g., pH and heat) in solution.[17] As such, the AMLO with liquidity can be advantageous over solid particles for applications such as controlled release and biosensing.

In this paper, we investigated a comprehensive list of possible cargoes for AMLOs, mirroring the versatility of natural MLOs. The list of cargoes included small molecules, proteins, DNAs, and RNAs. We measured the recruitment and release, and examined different triggers, namely, temperature, pH, and salt. Last, leveraging the AMLO's ability to concentrate fluorophores within the phase separated droplet, a temperature-sensitive aggregation-induced emission (AIE) sensor was constructed by manipulating the LLPS behavior of AMLO.

2. Results and Discussion

2.1. Enrichment of Multifaceted Cargoes from AMLO

The minimalist cationic AMLO harbors sites with multiple molecular interactions including electrostatic attraction, π–π and cation–π interactions,[15] having the potential to be carriers of a wide spectrum of cargoes (illustrated as Figure S1, Supporting Information). The AMLOs formed in intracellular

J. Liu, F. Zhorabek, Y. Chau
Department of Chemical and Biological Engineering
The Hong Kong University of Science and Technology
Clear Water Bay, Kowloon, Hong Kong SAR, P. R. China
E-mail: keychau@ust.hk
T. Zhang, J. W. Y. Lam, B. Z. Tang
Department of Chemistry and Hong Kong Branch of Chinese National Engineering Research Center for Tissue Restoration and Reconstruction
The Hong Kong University of Science and Technology
Clear Water Bay, Kowloon, Hong Kong SAR, P. R. China
B. Z. Tang
School of Science and Engineering
Shenzhen Key Laboratory of Functional Aggregate Materials
The Chinese University of Hong Kong, Shenzhen
Shenzhen City, Guangdong 518172, P. R. China
The ORCID identification number(s) for the author(s) of this article can be found under https://doi.org/10.1002/smll.202201721.

DOI: 10.1002/smll.202201721

physiological-mimicking buffer (IPM buffer, see Supporting Information) and fetal bovine serum (FBS) cell culture media, which can stabilize mostly up to 24 h (Figure S22, Supporting Information), with acceptable cell viability under sub-μM amount of incorporation (Figure S21, Supporting Information). We first investigated fluorescent small molecules, wherein enrichment of molecules was indicated by the enhancement of fluorescence intensity. Small fluorescent molecules, including fluorescein isothiocyanate (FITC), rhodamine B (RB), as well as fluorescent drugs, including riboflavin (Rib) and ellipticine, were recruited and highly enriched within AMLOs (**Figure 1**a and Figure S23, Supporting Information). By contrast, other fluorophores, including rhodamine 123 (R123) and doxorubicin (Dox), showed no appreciable enrichment (Figure S2, Supporting Information and Figure 1b). We also noticed a water-insoluble dye, Nile red, aggregated preferentially at the AMLO-water interfacial layer (Figure S3a, Supporting Information). All these data, summarized in Table S1, Supporting Information, suggest that the interior of AMLOs harbor some organic-solvent-like nature that is favorable for aromatic molecules. Similar organic-solvent-like nature was found in poly-lysine droplets enriching organic dyes and porphyrin,[18] as well as IDP droplets that can melt DNA double helix.[19]

We next investigated fluorophore-containing macromolecules. Two fluorophore-labeled hydrophilic macromolecules, RB-labeled 8 kDa polyethylene glycol (RB-PEG8k-OH) and FITC-labeled 40 kDa dextran (FITC-Dex40k), showed enrichment (Figure 1a), whilst larger macromolecules, such as

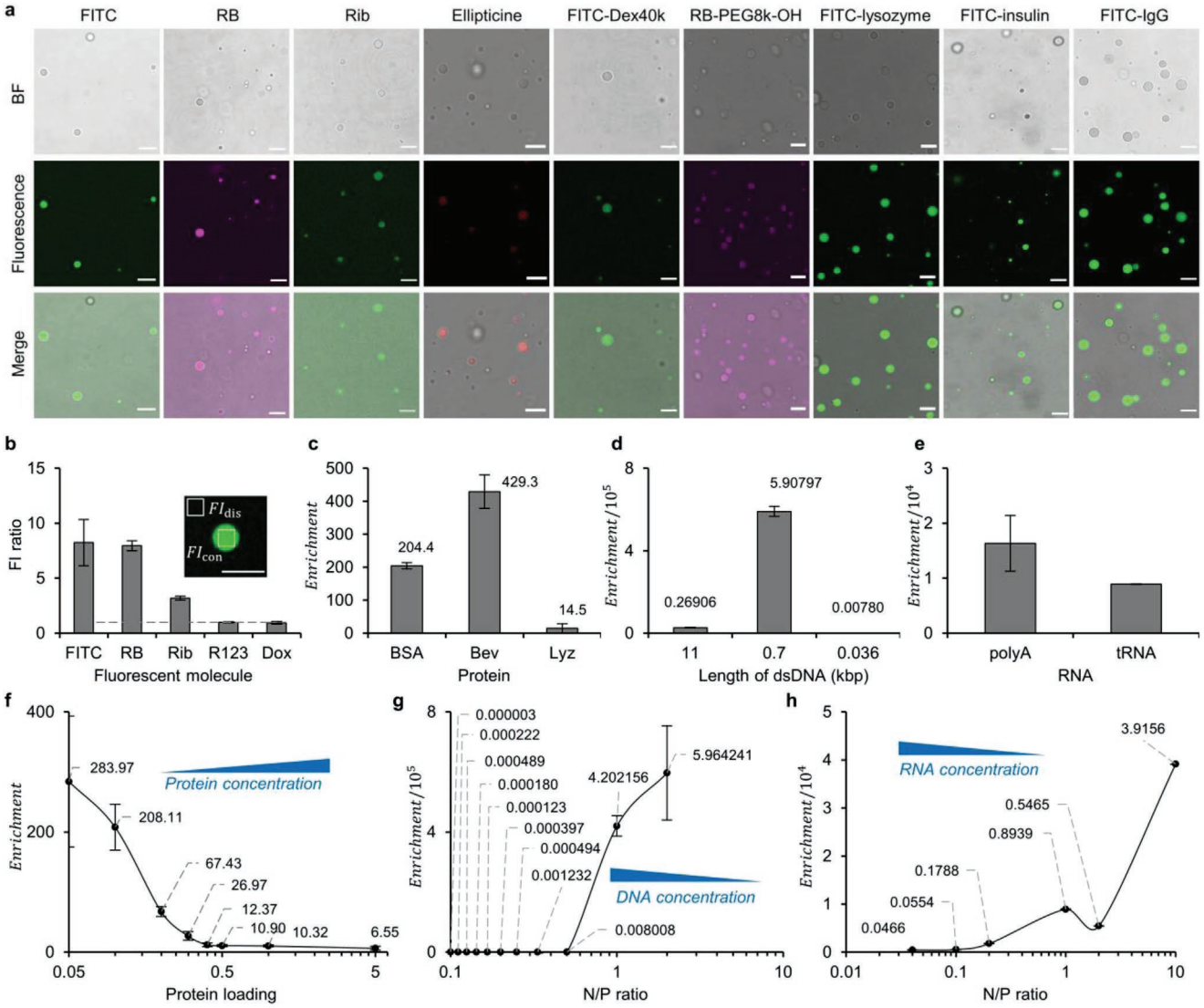

Figure 1. Enrichment of multifaceted cargoes in AMLOs. a) Enrichment of fluorescent molecules. Co-localization of high fluorescence intensity and droplet phase indicate enrichment of fluorescent cargo molecules. For concentrations, 8 μM was used for FITC, RB, and riboflavin, 100 μM was used for ellipticine, 60 μg mL^{-1} was used for FITC-Dex40k, RB-PEG8k-OH, FITC-lysozyme, FITC-insulin, and FITC-IgG. Scale bars, 10 μm. b) Enrichment of fluorescent molecules as indicated by FI ratio, and FI ratio = 1 (dashed line, no enhancement) was plotted for reference. Scale bar, 10 μm. c) Enrichment of protein, d) dsDNA, and e) RNA. Protein loading was 0.1, whilst dsDNA and RNA were loaded at N/P = 1. f) Stoichiometry-dependent loading of BSA, g) $dsDNA_{0.7kbp}$, and h) tRNA. $n = 3$.

FITC-Dex150k and FITC-Dex2000k, showed interfacial aggregation (Figure S3b, Supporting Information), presumably owing to size-based selection and exclusion. Three FITC-labeled proteins, namely, lysozyme, insulin, and immunoglobulin G (IgG), demonstrated enrichment within AMLOs (Figure 1a). Note that under physiological conditions, native lysozyme showed no preferential partitioning within AMLOs (Figure S16, Supporting Information, will be discussed later), thus suggesting the potential of fluorophores as molecular "drivers" for the localization of desired molecules.

We further investigated the enrichment of native biological compositional macromolecules of natural MLOs, including protein,[6] double-stranded DNA (dsDNA),[7] and RNA.[9,20–22] To quantify the AMLO system with cargo loaded, the discontinuous droplet (condensed) phase was separated from the continuous bulk (dispersed) phase by high-speed centrifugation, followed by quantification of concentration of cargoes in the supernatant (see Supporting Methods). Two model proteins, bovine serum albumin (BSA) and bevacizumab (Bev), were preferentially recruited and enriched over two orders of magnitude (Figure 1c), whilst lysozyme (Lyz) showed no appreciable enrichment under all stoichiometries incorporated (Figure S16, Supporting Information). Under physiological conditions, Lyz is strongly positively charged (pI = 11.35[23]), whilst BSA (pI = 5.1–5.5[24]) and Bev (pI = 8.3[25]) carry negative charge and slight positive charge, respectively. We reason that Lyz was not enriched owing to electrostatic repulsion, while BSA was enriched to over 200 folds owing to electrostatic attraction and/or aromatic interaction, and Bev was enriched to over 400 folds owing to aromatic interaction. BSA was also investigated under different loadings from 0.05 to 5, exhibiting distinct enrichment spanning from 284 to 6.55 (Figure 1f), suggesting the capacity of AMLO to preferentially partition proteins across a wide spectrum of stoichiometry.

Three model dsDNAs with varied lengths, namely, $dsDNA_{11kbp}$, $dsDNA_{0.7kbp}$, and $dsDNA_{0.036kbp}$, showed enrichment in an extremely prominent fashion (up to 10^5 enrichment, Figure 1d). Interestingly, the enrichment of dsDNAs tested is highly length-dependent, spanning over three orders of magnitude of enrichment ranging from 5.91×10^5 to 780 (Figure 1d). In addition, AMLOs enrich dsDNA in a highly stoichiometry-dependent fashion, wherein a small variation of N/P ratio from 1:1 to 1:2 generates over three orders of magnitude change of enrichment from 4.20×10^5 to 801 (Figure 1g). We reason electrostatic attraction is the predominant driving force of the enrichment of dsDNA within AMLOs, whereby dsDNA shows extremely high enrichment under charge complementary state, namely, N/P ratio equals 1:1. At a higher loading (N/P ratio = 1:2) of dsDNA, enrichment drops drastically owing to the limited charge attraction provided by AMLOs.

Two model RNAs, namely, polyA (2.3 kb) and tRNA (0.078 kb), demonstrated around 10^4 folds of enrichment within AMLOs (Figure 1e), presumably owing to the synergistic effect from electrostatic attraction and aromatic interactions (with nucleobases). In addition, increase of RNA loading by tuning N/P ratio from 1:0.1 to 1:25 resulted in decrease in enrichment from 3.92×10^4 to 466 (Figure 1h), showing the capacity of AMLO to enrich RNAs over a wide spectrum of stoichiometry.

We also observed distinct morphological changes in AMLOs with loading of different biomacromolecules. Sphericity was largely maintained with the loading of BSA (Figure S11, Supporting Information) and RNA (Figure S13, Supporting Information), whilst AMLOs solidified into irregular assemblies in the presence of dsDNAs, especially with longer dsDNA or at lower N/P ratio (Figure S12, Supporting Information). This can be explained by a combinational effect of chain stiffness of nucleic acids and strength of complexation. For one thing, compared with the double-stranded chains of DNAs,[26] the stiffness of the single-stranded chains of RNAs is distinctively lower. For another, charge densities of RNAs are lower than DNAs, which engender weaker electrostatic interactions and strength of complexation with the binding partner,[27] namely, polycationic IPH*.

2.2. Triggered Recruitment and Release of Biomolecules from AMLO

As natural MLOs are hubs of myriad biological molecules engaged with complex cellular metabolism, the compositional control is of vital importance.[12] We thus examined whether environmentally responsive AMLO[15] can achieve triggered recruitment or release of biomolecules, by studying two model biomolecules: BSA and dsDNAs. Three stimuli—temperature, pH, and ionic strength (salt concentration)—were investigated, owing to their relevance to physiology[28–31] and significant contributions to the phase behavior.[5]

We first investigated BSA, a model protein with good stability under investigated temperature[32] and pH[33] ranges. AMLO loaded with BSA exhibited highly responsive cargo release upon heating, releasing over 50% of BSA in response to 5 °C temperature increase with 5-min (Figure S17, Supporting Information) or 30-min (**Figure 2**a) incubation. The AMLOs also showed triggered recruitment of BSA upon cooling (Figure 2a). This can be explained by the upper critical solution temperature (UCST) phase behavior of IPH*,[15] wherein extent of LLPS is lower under higher temperature. Droplets with smaller volume fraction formed upon heating, thereby releasing cargoes encapsulated out of the condensed phase, and vice versa. The AMLOs exhibited prominent release of BSA upon acidification and showed recruitment upon alkalinization (Figure 2b). Under pH 7.4, BSA (pI = 5.1–5.5[24]) is negatively charged, whilst for IPH*,[15] arginines are the only charged sites (pK_a of side chain of arginine, 12.48[34]) with positive charges. IPH* stayed positively charged under the pH range investigated, whilst the charging state of BSA was modulated by pH. Acidification generated less electrostatic attraction. When pH was lower than pI, electrostatic repulsion led to the release of BSA. In contrast, alkalization generated stronger electrostatic attraction and triggered the recruitment of BSA. Increased ionic strength triggered release of BSA effectively, as is indicated by the complete release of BSA under 300 mM NaCl concentrations, owing to the weakened electrostatic interactions from electrostatic screening effect,[35] thus suggesting electrostatic attraction is the predominant driving force for the enrichment of BSA.

We further tested dsDNAs which were considered as stable under the conditions we used.[36] No appreciable recruitment

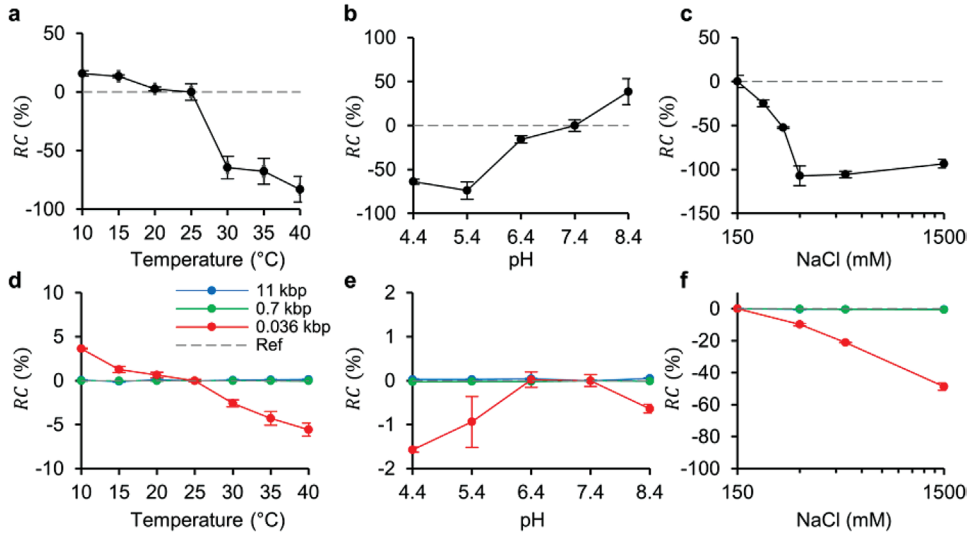

Figure 2. Triggered recruitment and release of cargoes from AMLOs. Recruitment/release of BSA triggered by a) temperature, b) pH, and c) salt. The concentrations of NaCl shown in (c) are 150, 200, 250, 300, 500, 1500 mM. Recruitment/release of DNA triggered by d) temperature, e) pH, and f) salt. The concentrations of NaCl shown in (f) are 150, 300, 500, 1500 mM. (e,f) share the same legend with (d). The "initial state" is 25 °C, pH = 7.4 and 150 mM NaCl for (a,d), (b,e) and (c,f), respectively. The BSA and dsDNAs were loaded at protein loading = 0.2 and N/P = 1, respectively. $n = 3$.

or release was observed for large dsDNAs (0.7 kbp and 11 kbp) under all temperature, pH or salt conditions tested, whereas apparent release was only observed for small dsDNA (0.036 kbp) under high salt concentrations (Figure 2d–f), thus suggesting a strong binding between dsDNA and IPH* harboring both electrostatic and aromatic interactions. The high stability of AMLO-dsDNA complex is consistent with the aforementioned ultrahigh enrichment of dsDNA within AMLOs (Figure 1d), as well as the formation of irregular assemblies in the presence of large dsDNAs (0.7 kbp and 11 kbp).

2.3. Controllable AIE from AMLOs

Unlike the conventional aggregation-caused quenching (ACQ) effect, AIE is a unique photophysical phenomenon wherein non-emissive luminogens were induced to emit intensely by aggregation.[37] The light emission of AIE luminogens (AIEgens) is strongly dependent on the aggregation state because it affects the extent of nonradiative decay by intramolecular motions.[38] Based on the minimalist AMLO system, we sought to leverage the LLPS phenomenon to rapidly and reversibly control AIE signal, through the recruitment and release of AIEgens.

We selected 1,2-bis[4-(4-sulfonatobutoxyl)phenyl]-1,2-diphenylethene salt (BSBOTPE) and Congo red as model luminescent dyes with AIE and ACQ attributes, respectively, while the two dyes have similar molecular weight, cationic nature, hydrophilicity and aromaticity (Figure S18, Supporting Information). The colocalization of fluorescence and AMLO confirmed the compartmentalization and enrichment of both dyes (Figure S18, Supporting Information). The overall fluorescence intensity of dye-loaded AMLO solution was quantified to investigate the light-emission of dyes (**Figure 3**). For Congo red, neither LLPS nor temperature demonstrated appreciable effect on the overall fluorescence intensity of solution under all concentrations tested (Figure 3a). By contrast, LLPS significantly enhanced the fluorescence of BSBOTPE in a temperature-responsive manner, whilst these LLPS-induced AIE and temperature-sensitivity were more prominent under higher dye concentrations (Figure 3b), owing to the higher extent of aggregation within the condensed phase. By comparison, without LLPS (Figure 3b, "in buffer"), the fluorescence of BSBOTPE exerted no significant change to temperature under all concentrations tested. The IPH* with UCST exhibited dye recruitment and release at lower and higher temperature, respectively, thereby modulating the aggregation state of AIEgens. As a result, the AIE effect is preferred at lower temperature (Figure 3b). We further studied the effect of extent of LLPS on AIE by modulating the concentration of IPH*. While the extent of LLPS generated no effect on the fluorescence of Congo red, LLPS exerted a drastic impact on the fluorescence of BSBOTPE in a high dose-dependent manner, which enhanced the fluorescence intensity by 34 folds at 54 μM IPH* incorporation (Figure 3c). This suggests the effective temperature-sensitive magnification of AIE. Moreover, at 54 μM IPH* incorporation, the AIE signal was attenuated to less than a thirtieth at 40 °C (Figure 3c), which was also demonstrated by the vanishing of fluorescence within 16 s at 40 °C (Figure S19 and Video S1, Supporting Information). This suggests the efficacious and rapid control of AIE by LLPS. The repeated heating-cooling thermo-cycling test (Figure S20a, Supporting Information) indicated the reversibility of LLPS-control of AIE signals (Figure S20b, Supporting Information). It was noted that upon heating-cooling cycling, the AIE signal regeneration was not totally complete. The fluorescence intensity regenerated 60.0%, 61.8%, and 47.1% of the original value after 1, 2, and 6 cycles of heating-cooling, respectively, presumably owing to the incomplete reversibility of LLPS of IPH*.[15]

3. Conclusion

A minimalist AMLO model system was capable of potent enrichment of different types of cargoes including small fluorescent dyes, small fluorescent drugs, fluorophore-containing

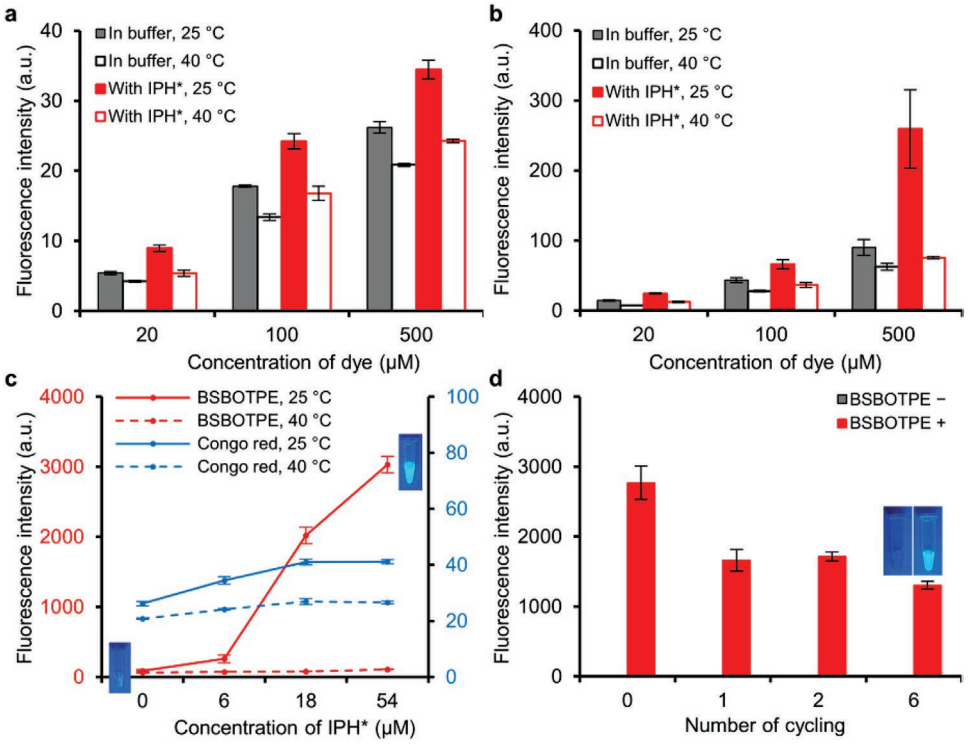

Figure 3. Controllable AIE by AMLOs. a,b) Concentration-dependent incorporation of a) Congo red and b) BSBOTPE. Either IPM buffer or 6 μM IPH* was used as the solvent. c) Incorporation of dyes at 500 μM under different extents of LLPS, which is controlled by the concentration of IPH*. d) Reversibility test by repeated heating-cooling cycling. The excitation/emission wavelengths used for Congo red and BSBOTPE are 497 nm/614 nm and 350 nm/500 nm, respectively. The insets are photographs of IPH* droplets without/with BSBOTPE taken under 365 nm illumination from the same UV lamp (UVGL-25, Analytik Jena, USA). $n = 3$.

macromolecules, proteins, DNAs, and RNAs. Triggered release by temperature, pH, and salt was demonstrated owing to the dynamic nature of the AMLO. Moreover, rapid and reversible control of AIE through temperature-responsive LLPS was attained. This simple yet versatile AMLO with liquidity is ideal for the enrichment and storage of biomolecules, as well as the dynamic, rapid, and reversible regulation thereof, which is advantageous over traditional solid particles. This minimalist AMLO is promising for the delivery of biomolecules or drugs into cells, as well as the efficient removal of charged or aromatic pollutants in aqueous solution.

4. Experimental Section

This part is provided in the Supporting Information.

Supporting Information

Supporting Information is available from the Wiley Online Library or from the author.

Acknowledgements

Financial support was provided by the Hong Kong Research Grant Council (GRF 16102520 and GRF 16103517), the Innovation and Technology Commission (ITC CNERC14SC01), and the Hong Kong Ph.D. Fellowship Scheme (for Jianhui Liu).

Conflict of Interest

The authors declare no conflict of interest.

Data Availability Statement

The data that support the findings of this study are available in the supplementary material of this article.

Keywords

aggregation-induced emission, artificial, liquid-liquid phase separation, membraneless organelles, recruitment and release

Received: March 18, 2022
Revised: April 15, 2022
Published online: May 21, 2022

[1] A. Honigmann, A. Pralle, *J. Mol. Biol.* **2016**, *428*, 4739.
[2] S. F. Banani, H. O. Lee, A. A. Hyman, M. K. Rosen, *Nat. Rev. Mol. Cell Biol.* **2017**, *18*, 285.

[3] A. A. Hyman, C. A. Weber, F. Jülicher, *Annu. Rev. Cell Dev. Biol.* **2014**, *30*, 39.
[4] J. R. Espinosa, J. A. Joseph, I. Sanchez-Burgos, A. Garaizar, D. Frenkel, R. Collepardo-Guevara, *Proc. Natl. Acad. Sci. USA* **2020**, *117*, 201917569.
[5] K. K. Nakashima, M. A. Vibhute, E. Spruijt, *Front. Mol. Biosci.* **2019**, *6*, 21.
[6] S. C. Weber, C. P. Brangwynne, *Cell* **2012**, *149*, 1188.
[7] J. T. King, A. Shakya, *Biophys. J.* **2021**, *120*, 1139.
[8] M. Polymenidou, *Science* **2018**, *360*, 859.
[9] K. Rhine, V. Vidaurre, S. Myong, *Annu. Rev. Biophys.* **2020**, *49*, 247.
[10] J. A. Ditlev, L. B. Case, M. K. Rosen, *J. Mol. Biol.* **2018**, *430*, 4666.
[11] H. Y. J. Fung, M. Birol, E. Rhoades, *Curr. Opin. Struct. Biol.* **2018**, *49*, 36.
[12] S. F. Banani, A. M. Rice, W. B. Peeples, Y. Lin, S. Jain, R. Parker, M. K. Rosen, *Cell* **2016**, *166*, 651.
[13] N. A. Yewdall, A. A. M. André, T. Lu, E. Spruijt, *Curr. Opin. Colloid Interface Sci.* **2021**, *52*, 101416.
[14] J. Liu, F. Zhorabek, Y. Chau, *arXiv2104.10927* **2021**.
[15] J. Liu, F. Zhorabek, X. Dai, J. Huang, Y. Chau, *ACS Cent. Sci.* **2022**, *8*, 493.
[16] J. Liu, F. Zhorabek, Y. Chau, *ACS Macro Lett.* **2022**, *32*, 562.
[17] S. Alberti, A. Gladfelter, T. Mittag, *Cell* **2019**, *176*, 419.
[18] S. Koga, D. S. Williams, A. W. Perriman, S. Mann, *Nat. Chem.* **2011**, *3*, 720.
[19] T. J. Nott, T. D. Craggs, A. J. Baldwin, *Nat. Chem.* **2016**, *8*, 569.
[20] C. Roden, A. S. Gladfelter, *Nat. Rev. Mol. Cell Biol.* **2021**, *22*, 183.
[21] A. Drino, M. R. Schaefer, *BioEssays* **2018**, *40*, 1800085.
[22] E. M. Langdon, A. S. Gladfelter, *Annu. Rev. Microbiol.* **2018**, *72*, 255.
[23] L. R. Wetter, H. F. Deutsch, *J. Biol. Chem.* **1951**, *192*, 237.
[24] D. Fologea, B. Ledden, D. S. McNabb, J. Li, *Appl. Phys. Lett.* **2007**, *91*, 053901.
[25] S. Kaja, J. D. Hilgenberg, E. Everett, S. E. Olitsky, J. Gossage, P. Koulen, *Hum. Antibodies* **2011**, *20*, 95.
[26] A. Shakya, J. T. King, *Biophys. J.* **2018**, *115*, 1840.
[27] J. R. Vieregg, M. Lueckheide, A. B. Marciel, L. Leon, A. J. Bologna, J. R. Rivera, M. V. Tirrell, *J. Am. Chem. Soc.* **2018**, *140*, 1632.
[28] T. J. Nott, E. Petsalaki, P. Farber, D. Jervis, E. Fussner, A. Plochowietz, T. D. Craggs, D. P. Bazett-Jones, T. Pawson, J. D. Forman-Kay, A. J. Baldwin, *Mol. Cell* **2015**, *57*, 936.
[29] M. Hondele, R. Sachdev, S. Heinrich, J. Wang, P. Vallotton, B. M. A. Fontoura, K. Weis, *Nature* **2019**, *573*, 144.
[30] Y. Lu, T. Wu, O. Gutman, H. Lu, Q. Zhou, Y. I. Henis, K. Luo, *Nat. Cell Biol.* **2020**, *22*, 453.
[31] G. L. Dignon, W. Zheng, Y. C. Kim, J. Mittal, *ACS Cent. Sci.* **2019**, *5*, 821.
[32] A. Michnik, *J. Therm. Anal. Calorim.* **2003**, *71*, 509.
[33] L. R. S. Barbosa, M. G. Ortore, F. Spinozzi, P. Mariani, S. Bernstorff, R. Itri, *Biophys. J.* **2010**, *98*, 147.
[34] M. Evich, E. Stroeva, Y. G. Zheng, M. W. Germann, *Protein Sci.* **2016**, *25*, 479.
[35] L. M. Jawerth, M. Ijavi, M. Ruer, S. Saha, M. Jahnel, A. A. Hyman, F. Jülicher, E. Fischer-Friedrich, *Phys. Rev. Lett.* **2018**, *121*, 258101.
[36] B. Shieh, I. J. Su, W. J. Chuang, C. Li, *BioTechniques* **1998**, *24*, 60.
[37] J. Mei, N. L. C. Leung, R. T. K. Kwok, J. W. Y. Lam, B. Z. Tang, *Chem. Rev.* **2015**, *115*, 11718.
[38] H. Wang, E. Zhao, J. W. Y. Lam, B. Z. Tang, *Mater. Today* **2015**, *18*, 365.